Zou et al. BMC Biology (2025) 23:103
https://doi.org/10.1186/s12915-025-02212-z

BMC Biology

RESEARCH ARTICLE Open Access

High-fat diet alters retinal lipid composition and gene expression networks in mice

Rong Zou[1†], Jinrui Cai[1†], Tianyu Chen[1], Wenhui Mo[1], Hao Qian[1*], Xianjun Zhu[1,2,3*] and Lin Zhang[1,3*]

Abstract

Background High-fat diet (HFD) was suggested to be associated with several retinal diseases, including age-related macular degeneration (AMD), glaucoma, and diabetic retinopathy (DR). Nevertheless, our understanding of the mechanisms governing retinal lipid metabolic homeostasis remains limited, with little attention focused on the influence of HFD on different retinal cell types. To address this gap, we established a high-fat model using mice fed with HFD for a duration of 6 months. Then, we conducted a comparative analysis of the retinal lipidome and proteome between normal diet (ND) and HFD-fed mice to explore the impacts of HFD on retinal lipid metabolism and gene expression network. Furthermore, we also investigated the impacts of HFD on retina in single-cell resolution by single-cell transcriptome sequencing.

Results We found that a long-term HFD significantly altered the lipid composition of the retina, with a dramatically elevated cholesterylesters (CE), phosphatidylcholine (PC), and phosphatidylglycerol (PG) level and a decreased eicosanoid level. Proteomic analysis revealed that the primary bile acid biosynthesis pathway was over-activated in HFD retinas. By using single-cell transcriptome analysis, we identified different regulation of gene expression in MG and rod cells in a high-fat environment, whereas the previously identified activation of the bile acid synthesis pathway was predominantly found in MG cells, and may be regulated by alternative pathways of bile acid synthesis, suggesting the critical roles of MG cells in retinal lipid metabolism.

Conclusions Taken together, by multi-omics studies, we unveiled that HFD leading to the development of retinal diseases may be regulated by alternative pathways of bile acid synthesis, and our study will shed light on the treatment of these diseases.

Keywords HFD, Metabolic homeostasis, Retina, Cholesterol

†Rong Zou and Jinrui Cai contributed equally to this work.

*Correspondence:
Hao Qian
qianhao@uestc.edu.cn
Xianjun Zhu
xjzhu@uestc.edu.cn
Lin Zhang
zhanglin202@uestc.edu.cn
[1] The Sichuan Provincial Key Laboratory for Human Disease Gene Study, Center for Medical Genetics, Sichuan Provincial People's Hospital, School of Medicine, University of Electronic Science and Technology of China, Chengdu, Sichuan 610072, China
[2] Henan Branch of National Clinical Research Center for Ocular Diseases, Henan Eye Hospital, People's Hospital of Zhengzhou University, Henan Provincial People's Hospital, Zhengzhou, China
[3] Qinghai Provincial Key Laboratory of Tibetan Medicine Research, Northwest Institute of Plateau Biology, CAS, Xining, Qinghai 810008, China

Background

The eye is the main organ through which we perceive the world. However, globally, at least 2.2 billion people are visually impaired [1, 2]. This causes immense suffering to patients and their families, and places a heavy burden on society, with an estimated global productivity loss of about $411 billion per year [3]. The retina is situated in the inner layer of the eye wall, bordered by the vitreous humor on its inner surface and the choroid on its outer surface. It exhibits a highly complex, multilayered structure, composed of numerous cell types with distinct microcircuit characteristics and specialized functions. These cellular components are essential for visual processing, as they are responsible for detecting and processing incoming light to generate visual signals, which are subsequently transmitted to the brain via the optic nerve [4]. The normal retina has a clear structure with distinct boundaries of each layer, which mainly consists of retinal pigment epithelial cells (RPE), photoreceptor cells, bipolar cells, ganglion cells, horizontal cells, amacrine cells, and MG cells [5]. Degeneration or dysfunction of these cells is associated with different retinal diseases.

Lipids are important organic compounds in organisms and are widely found in plant and animal cells. According to their structure and function, they can be categorized into fatty acids, triglycerides, fatty acid phospholipids, steroids, and sphingolipids and so on [6]. Lipids in the retina serve as integral components of cell membranes and play crucial roles in various physiological processes, including the transduction of light signals, cellular protection, and energy metabolism. Disruptions in lipid metabolism can result in the onset and progression of a range of retinal disorders [7, 8].

Due to the blood-retina barrier (BRB), the eye, as a relatively independent organ, has a high degree of autonomy in its metabolism. A number of studies have now found retina-related diseases also associated with HFD [9]. For example, the current study found that glaucoma is associated with abnormal retinal lipid metabolism and that patients with primary open-angle glaucoma (POAG) have lower expression of cholesterol transport-associated protein (ABCA1) as well as lower serum levels of high-density lipoproteins (HDL) [10]. *Abca1* knockout mice present a glaucoma-like phenotype with massive RGC death and symptoms identical to those of patients with POAG. And the symptoms of POAG mice were alleviated after the use of atorvastatin (ATOR) [11]. Studies from several other groups proved an association between hyperlipidemia and POAG [9, 12–14]. However, these findings are contradictory, some studies have reported a reduced risk of POAG in patients with hyperlipidemia, while others have found a positive correlation between hyperlipidemia and POAG risk [15–17]. Also controversial is the fact that some findings have proven ATOR to be effective in the treatment of glaucoma, while others have proven it to be ineffective [10, 18, 19]. These results make the relationship between lipid metabolism and glaucoma elusive. Another retinal disease related to lipid metabolism is age-related macular degeneration (AMD), which is one of the common causes of blindness and mainly affects the elderly population. It has been found that patients with AMD are often associated with hyperlipidemia as well as the presence of lipid accumulation in drusen in the choroid [20]. Excessive LDL accumulation was found in the retinas of HFD-fed mice after apolipoprotein E (ApoE) deletion, and the ApoE deletion mice show a phenotype of AMD, including RPE degeneration, hyperpigmentation, and photoreceptor dysfunction [21–24]. In addition to these two seriously damaging diseases, recent studies have shown an association between HFD and the onset and progression of retinitis pigmentosa (RP) [25–27]. It has been shown that short-term HFD induces hyperglycemia and metabolic syndrome and exacerbates RP [28]. After specific deletion of *rlbp1b* in zebrafish RPE and MG cells, cone photoreceptors were found to be functionally and metabolically compromised and manifested as enlarged lipid droplets in the retina [26]. In addition to the studies on the relationship between lipid metabolism and retinal disease, additional studies have shown that a high-fat diet has physiologic or functional effects on different parts of the eye, such as causing higher number of lesions in the RPE, decreased number of RPE, increased microglia activity, decreased ganglion cell function, and increased oxidative stress in the lens [9].

However, there is a lack of systematic studies on the mechanisms of regulation of metabolic homeostasis in the retina, and no attention has been paid to the effects HFD on different cells of the retina. To achieve this objective, we developed a HFD mouse model for conducting lipidomic, proteomic, and single-cell transcriptome analyses. Our investigation revealed that prolonged exposure to an HFD led to significant alterations in the lipid profile of the retina, notably demonstrating increased levels of CE, PC, and PG, alongside reduced eicosanoid levels. Furthermore, we determined that the primary bile acid biosynthesis pathway exhibited increased activity within HFD retinas. Additionally, we observed distinct patterns of gene expression regulation in MG cells and rod cells under high-fat conditions. Notably, the enhanced activation of the bile acid synthesis pathway was predominantly associated with MG cells, highlighting their critical role in retinal lipid metabolism. The insights derived from this study are expected to provide valuable guidance for the future management of lipid-related retinal disorders.

Results

High-fat diet mouse model construction

To investigate the effects of a HFD on retinal metabolic homeostasis and gene expression networks, we divided 6-week-old wild-type C57BL/6 J mice into two groups, and then fed a high-fat chow diet and a normal chow diet for 6 months, respectively. After feeding the mice with high-fat chow for 14 weeks, it was found that there was a significant difference in body size between HFM and NM (Supplementary figure S1-A-B), and the body weight of high-fat diet mice (HFM) began to be significantly higher than that of normal diet mice (NM), and HFM was almost 1.8 times of that NM after feeding for 32 weeks. In addition, HFM developed a fatty liver phenotype, characterized by an increase in liver size compared to NM group. The liver exhibited a yellowish appearance, with blunted edges and a greasy texture (Supplementary figure S1-C). Furthermore, the liver-to-body weight ratio was found to be elevated (Supplementary figure S1-D). Hematoxylin and eosin (H&E) staining results also showed lipid droplet accumulation in the HFM liver (Supplementary tab S1-E). Taken together, these results indicate the successful establishment of a HFD mouse model, which exhibited characteristic features of metabolic diseases, including obesity and fatty liver.

HFD did not lead to significant changes in retinal structure and function in mice

To assess whether a long-term HFD has an effect on retinal structure and function, we carried out OCT and ERG assays in HFM and NM mice, respectively. Upon examination using OCT, we observed no significant differences in retinal structure or thickness between the HFM and NM retinas (Fig. 1A). ERG analyses showed no differences in scotopic response between HFM and NM, indicating the overall photoreceptor function were not impaired after a long-term HFD (Fig. 1B).

Long-term HFD changes retinal lipid composition in mice

To investigate whether a long-term HFD would have an effect on the lipid composition of the retina, we analyzed the lipidome of the retinas of HFM and NM mice, respectively. The composition of lipids is tissue-specific, and samples from different tissues contain different lipid classes and proportions. We first assessed the overall composition and relative proportions of various lipid subclasses in the retina from NM and HFM. As shown in the radar charts, the proportion of each subclass to the total lipids was almost the same in the two groups (Fig. 2A). Specific to each lipid, by lipidomic analysis, a total of 1059 lipids were detected, of which 162 were upregulated and 40 were downregulated (fold change (FC) ≥ 1.2 or FC ≤ 0.8; variable importance in projection (VIP) ≥ 1; P-value < 0.05) in HFM retinas compared to NM retinas (Fig. 2B, table S1). In order to show the overall metabolic differences more clearly and intuitively, the FC values of the lipids in the two groups were calculated, and the lipids were ranked from smallest to largest according to the FC values. The dynamic distribution of the differences in lipid content was plotted, and the top 10 lipids were labeled for upregulation and downregulation. The lipids with the most significant upward changes are PC, free fatty acid (FFA), lyso-phosphatidylethanolamine (LPE), CE, and phosphatidylethanolamine (PE) (Fig. 2C).

In order to give a clearer profiling of the changed lipids in HFM retinas, we selected the top 50 mostly changed for further analyses. As shown in the heatmap, of the 50 lipids, the majority of which were elevated in HMF retina, with 15 lipids downregulated (Fig. 3A). We then categorized all identified differential lipids into different subclasses for quantitative analysis and found that 9 of these subclasses were elevated and 1 was decreased (Fig. 3B).

Subsequently, we performed KEGG pathway enrichment analysis on the significantly differentially expressed lipids between the NM and HFM groups. In the KEGG-enriched pathways of differential metabolites, the color of the dots represents the corresponding P-value. The size of the dots indicates the number of differentially enriched lipids. KEGG enrichment analysis showed that the most changed signaling are arachidonic acid metabolism, glycerophospholipid metabolism, and α-linolenic acid metabolism pathways (Fig. 4A). Sankey chart showed the relationships of these enriched pathways with organismal system, human diseases, cellular processes, metabolism, and environmental information processing (Fig. 4B). Taking these results together, we found that HFD ingestion altered the lipid composition and cellular function of the mouse retina, which may have contributed to the inflammation development and impaired synthesis of lipids such as cholesterol and phospholipids. But its exact effects and regulatory mechanisms need to be further explored.

Proteomics reveals significantly different gene expression alterations in retina with an HFD

To reveal whether a long-term HFD alters gene expression levels in the retina, we used 4D-label free mass spectrometry to quantify proteins in the whole retinas of HFM and age-mated NM [29]. As the liver plays a crucial role in metabolism of the whole body, HFD has a huge impact on gene expression in the liver. To compare the similarities and differences in the effects of a HFD on retinal and hepatic gene regulatory networks, we also performed proteomic analyses on the livers from HFM and

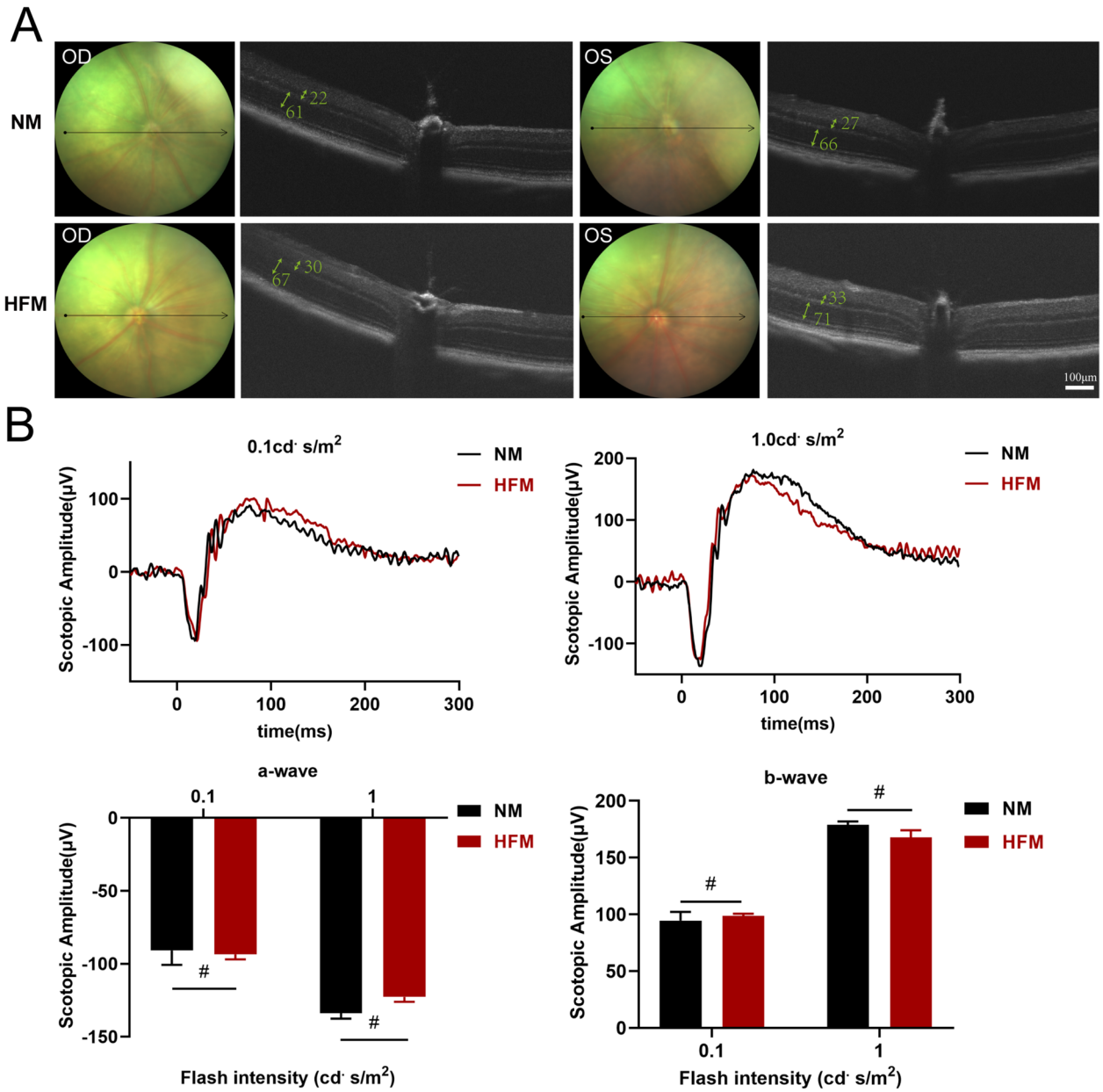

Fig. 1 HFD did not lead to significant changes in retinal structure and function in mice. **A** Fundus images and OCT scans of NM and HFM mice. Scale bar, 100 μm. **B** ERG traces corresponding to responses elicited by scotopic conditions at fash intensities of 0.1 and 1.0 cd·s/m^2 in mice at 6 months of age. Statistical analysis was performed for the amplitudes of the a-wave and b-wave under scotopic conditions ($n = 4$, unpaired *t*-test), #, no signifcant diference. Bars represent mean ± SEM

NM. As the results, a total of 38 differentially expressed proteins (DEPs) were identified in the HFM retinas compared to the NM retinas, of which 18 DEPs were downregulated and 20 DEPs were upregulated (Fig. 5A, table S2). Heatmap showed the top- 10 most down- and upregulated DEPs in retinas from HFM compared to NM (Fig. 5B). On the other hand, the DEPs between livers from HFM and NM are much more, with a total of 359 DEPs, of which 165 proteins were downregulated and 194 proteins were upregulated (Figure S2 A, table S3). A comparison of the DEPs in the retina and the liver revealed that there were only 4 identical hits between them, which were APOA4, MSH2, YIF1 A, and SERPINA3 K (Figure S2B-C). The overall profiling of gene expression maps from retina and liver demonstrated that HFD has a much smaller effect on the gene expression network in the

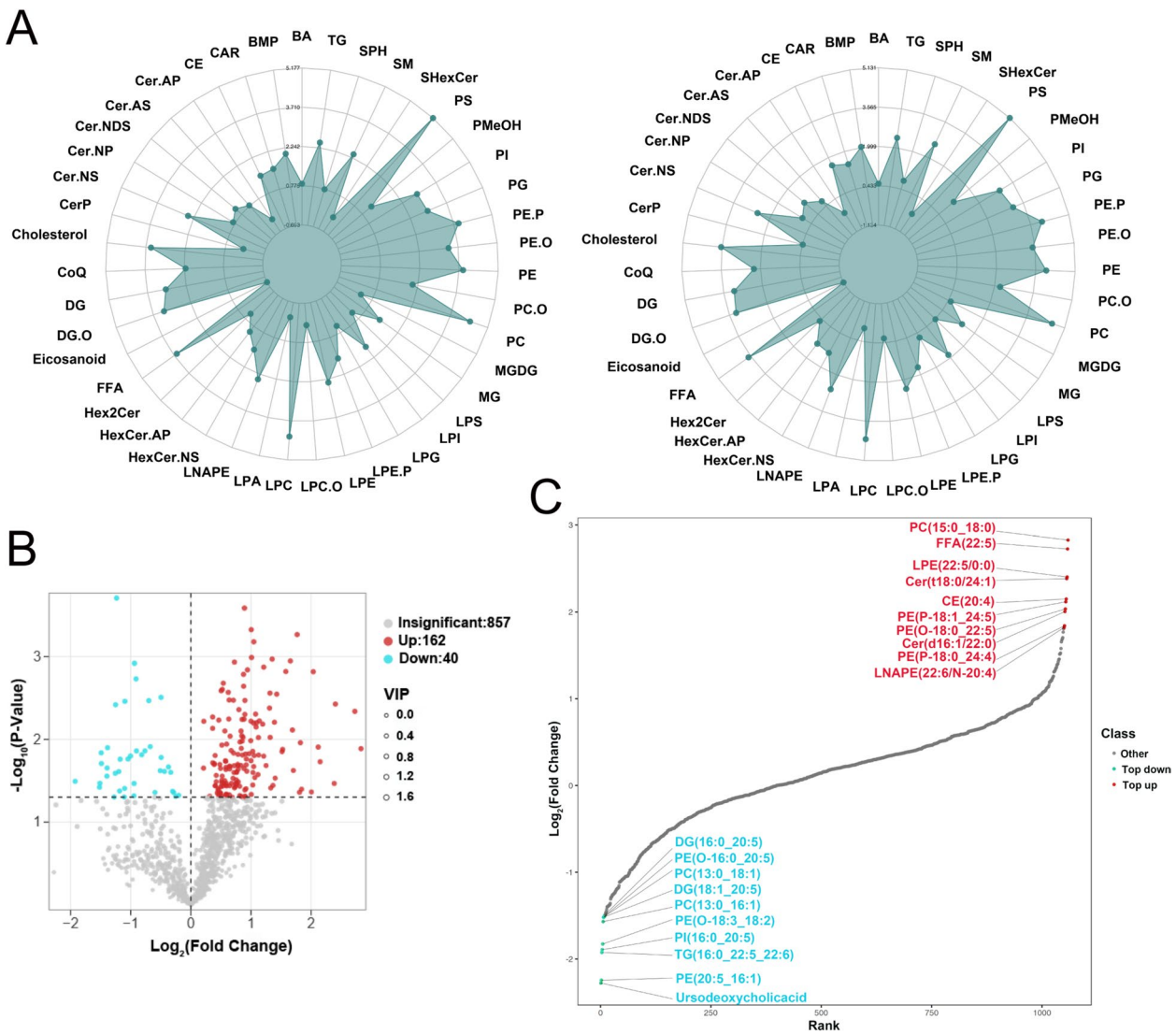

Fig. 2 Long-term HFD changes retinal lipid composition in mice. **A** Radar plots shows the overall composition and proportions of different subclasses of lipids in NM and HFM retinas. **B** Volcano map shows 1059 detected lipids, of which 162 were upregulated and 40 were downregulated (fold change (FC) ≥ 1.2 or FC ≤ 0.8; variable importance in projection (VIP) ≥ 1; *P*-value < 0.05) in HFM retinas compared to NM retinas. **C** The dynamic distribution plot demonstrates the differences in lipid content and labels the top 10 lipids that are upregulated and downregulated ($n = 3$)

retina compared to the liver, and that the corresponding patterns of the retina and the liver in response to HFD were different. Of the 4 proteins consistently altered in both retina and liver, APOA4 was the mostly markedly increased. The well-known function of APOA4 is that constructing the major component of HDL and chylomicrons, and involved in the catabolism of chylomicrons and VLDL [30]. A small number of studies have suggested that aberrant APOA4 expression may be associated with Alzheimer's disease, but the function of which in the retina has not been reported [30–33]. Our results suggested that elevated levels of APOA4 expression in a high-fat environment may play a role in protecting the retina from damage and could serve as a target for retinal disease therapy. We also noticed that, the MSH2, which is one of the components of the post-replicative DNA mismatch repair system, also overexpressed in the HFM retinas [34], indicating that a long-term HFD may have caused DNA damage to the retina. SERPINA3 K, a member of the serine protease inhibitor family and a novel class of Wnt signaling pathway inhibitors with anti-oxidative stress, anti-inflammatory, and anti-vascular effects in the fundus [35], was decreased in both retina and liver of HFD-fed mice.

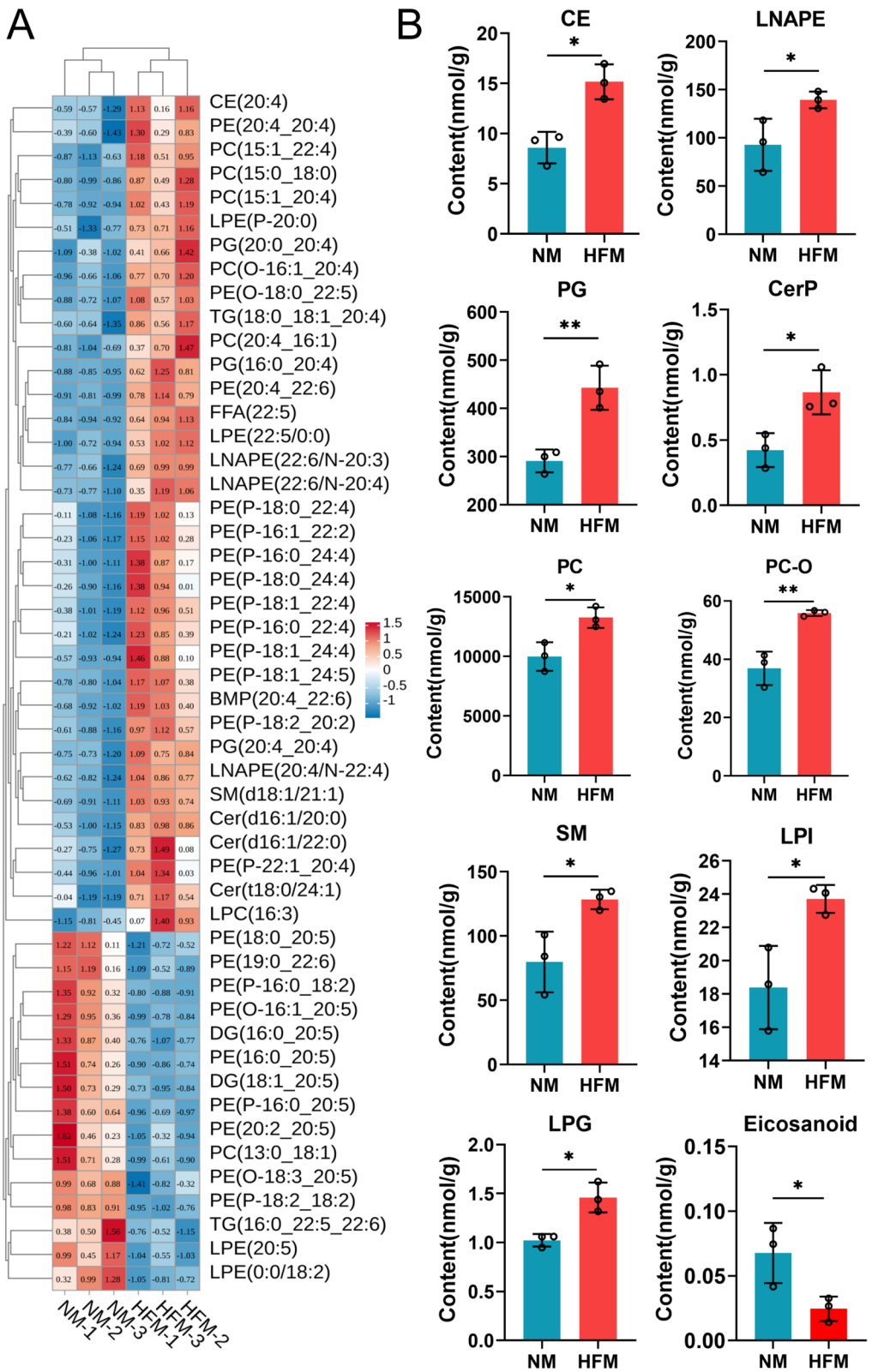

Fig. 3 Long-term HFD alters lipid subclass composition in mouse retina. **A** The heat map shows the top 50 lipids that changed ($n = 3$). **B** All identified differential lipids were divided into different subclasses for quantitative analysis and 9 of them were found to be elevated and 1 was found to be decreased. ($n = 3$, unpaired *t*-test), $^{*}P < 0.05$;$^{**}P < 0.01$. Bars represent mean ± SEM

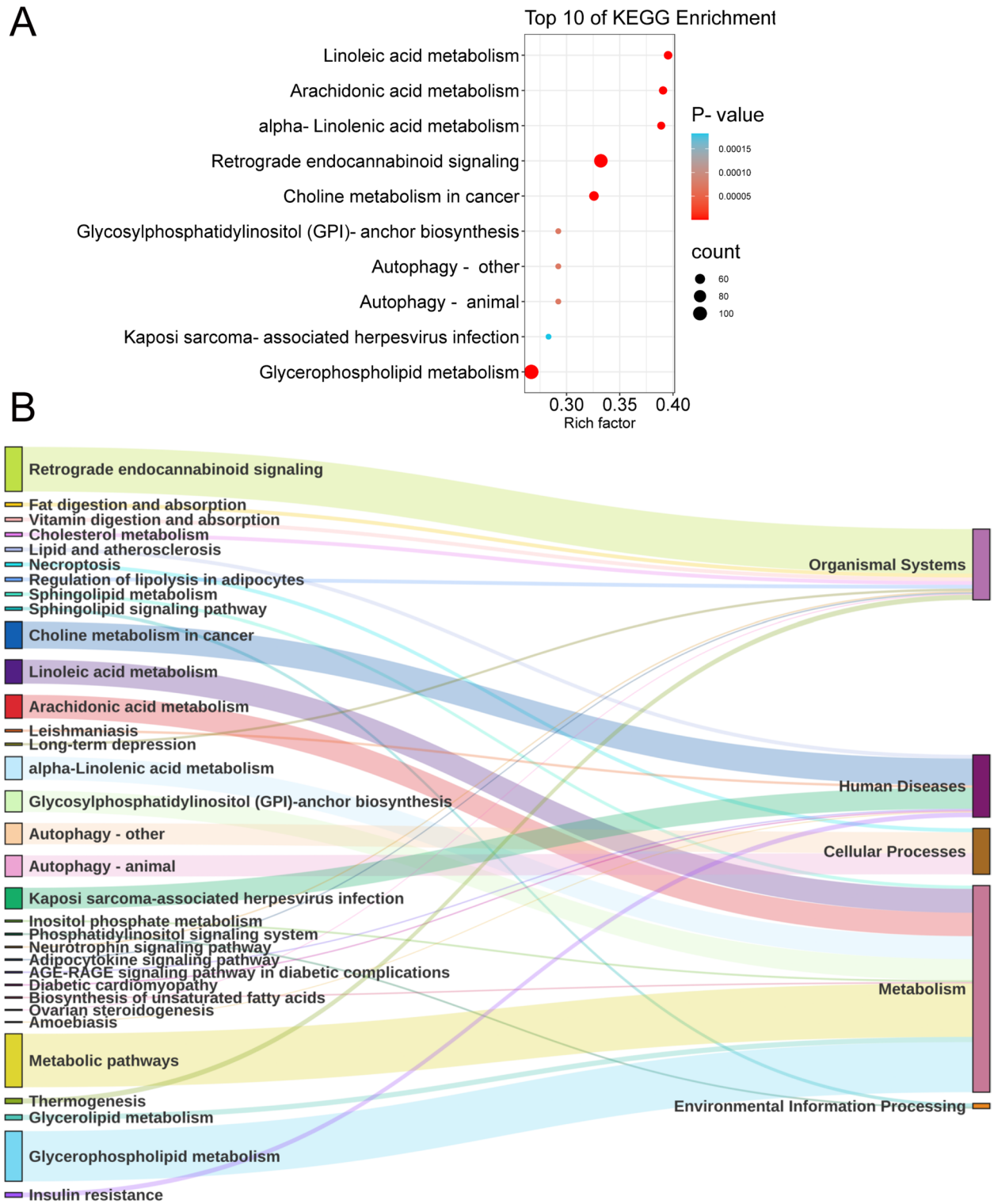

Fig. 4 Long-term HFD affects the regulatory network of retinal lipids. **A** KEGG pathway analysis of the differential lipids enriched in different pathways, showing the top 10 ranked pathways. **B** Sankey chart showed the relationships of these enriched pathways with organismal system, human diseases, cellular processes, metabolism, and environmental information processing

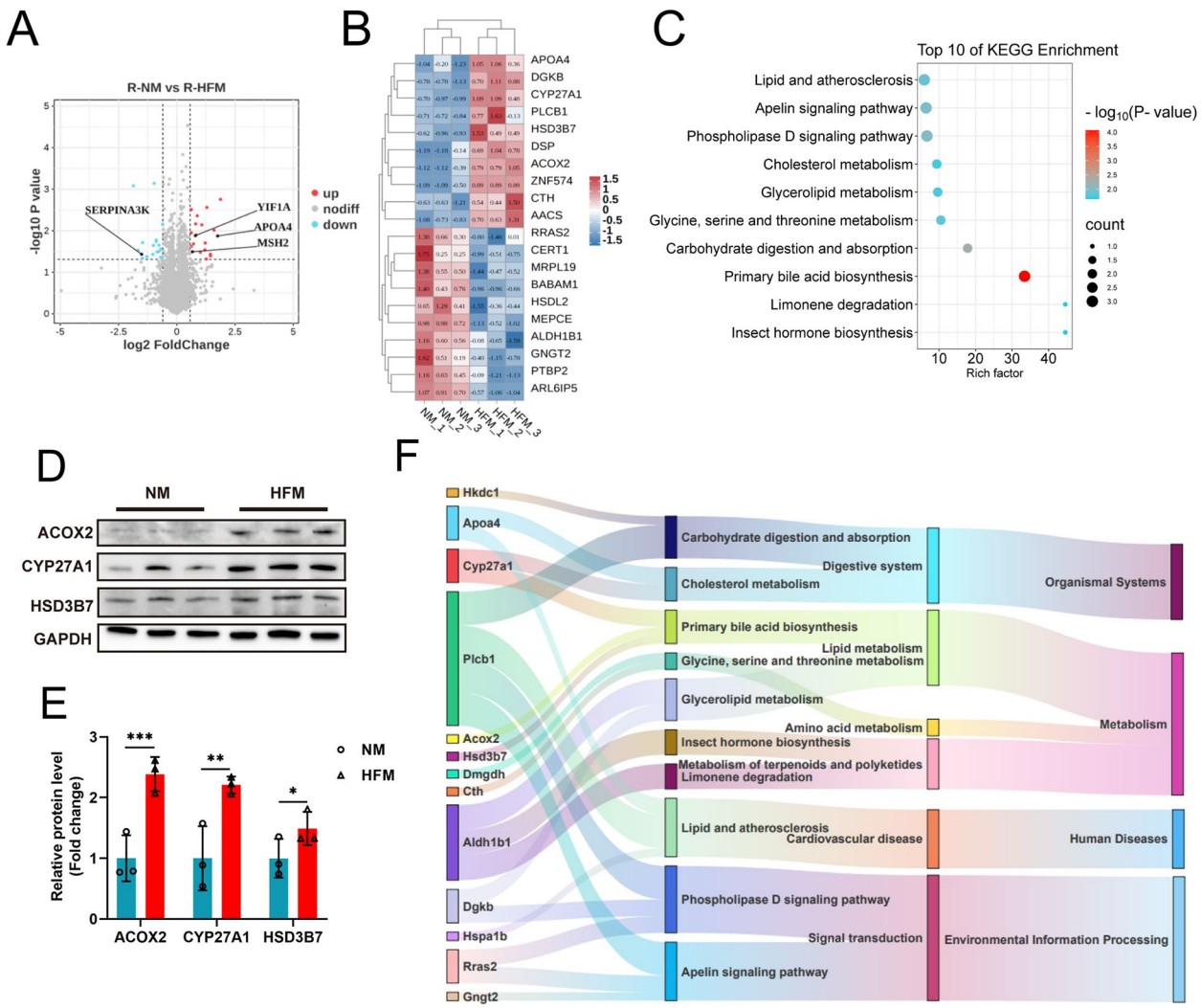

Fig. 5 Proteomics reveals significantly different gene expression alterations in retina with an HFD. **A** The volcano map shows a total of 38 differentially expressed proteins (DEPs) were identified in the HFM retinas compared to the NM retinas, of which 18 DEPs were downregulated and 20 DEPs were upregulated. **B** Heatmap showed the top- 10 most down- and upregulated DEPs in retinas from HFM compared to NM ($n = 3$). **C** KEGG pathway analysis of the DEPs enriched in different pathways, showing the top 10 ranked pathways. **D** Expression of proteins involved in the primary bile acid biosynthesis pathway in the retinas of 6-month-old NM and HFM ($n = 3$). **E** The panel shows the quantification of the proteins expression levels. The expression of each protein was normalized to that of GAPDH. ($n = 3$, unpaired *t*-test), $^{*}P < 0.05$; $^{**}P < 0.01$; $^{***}P < 0.001$. Bars represent mean ± SEM. **F** Sankey chart showed the relationship between the DEPs and KEGG pathways

Next, KEGG pathway analysis revealed that the DEPs in retina were mainly clustered into metabolism pathways, including lipid and atherosclerosis, phospholipase D signaling, cholesterol, and glycerolipid metabolism (Fig. 5C). We examined protein expression in the retina after HFD and showed that upregulation of three proteins of the primary bile acid biosynthesis pathway, ACOX2, CYP27 A1, and HSD3B7, which is consistent with the proteomic results (Fig. 5D–E). Sankey chart showed the relationship between the DEPs and KEGG pathways (Fig. 5F). For the liver, we also showed the top 10 most down- and upregulated DEPs in the heatmap, almost complete different to the retina (Figure S2D). Analysis of KEGG pathway enrichment of the DEPs in liver revealed that, unlike in the retina, a number of DEPs were enriched in "chemical carcinogenesis" and "PPAR signaling" pathways, indicating a long-term HFD have significant damage to the liver (Figure S2E).

Single-cell RNA transcriptome analysis

To explore the effects of HFD on different cells of the retina, we further carried out single-cell RNA sequencing analysis [36]. Through clustering analysis, we found that the samples from the two groups of NM and HFM

were mixed and clustered well, and the RPE, Rod, RGC, MG, Microglia, Horizon-Amacrine, Cone, and Bipolar were detected, with the highest percentage of Rod cells, followed by MG and Bipolar (Fig. 6A). The marker genes for each cell used are shown in the heat map (Fig. 6B).

We also analyzed the effects of HFD on gene expression of different cells. We first checked the most changed genes screened out by the proteomic analyses and found that *Dsp*, *Hsdl2*, and *Cth* were significantly upregulated; however, *Aacs*, *Ptbp2*, *Babam1*, and *Mepce* were significantly downregulated in the RPE cells. In MG, *Acox2*, *Dgkb*, and *Cyp27a1* were significantly upregulated, and the most altered genes screened by proteomic analysis were altered in different cells, suggesting that these genes are indeed involved in the metabolic regulation of the retina, but their regulatory mechanisms need to be further explored (Fig. 7A). In particular, we focused on three proteins of the proteomic KEGG-enriched primary bile acid biosynthesis pathway: Acox2, Cyp27a1, and Hsd3b7, and found that all three proteins were upregulated in MG, suggesting that cholesterol degradation after HFD may be associated with MG cells (Fig. 7B).

We next made KEGG pathway enrichment analyses on the differentially expressed genes (DEGs) in the MG and rod cells. In MG cells, the DEGs mainly enriched in glutamatergic synapse, axon guidance and pathways related to cell apoptosis, proliferation and inflammation, including Ras signaling pathway, MAPK signaling pathway, PI3 K-Akt signaling pathway, and Rap1 signaling pathway (Fig. 7C). While in rod cells, the DEGs mainly focused on protein synthesis-related pathways, including ribosome, spliceosome and protein processing in endoplasmic reticulum. KEGG pathways analysis results also showed that DEGs focused on metabolism pathways, including oxidative phosphorylation, thermogenesis, and lipid and atherosclerosis (Fig. 7D). Chord diagram shows the relationship between DEGs and KEGG pathways (Fig. 7E, F).

Discussion

Many retinal diseases, including glaucoma and AMD, are closely linked to lipid metabolism, and the pathogenic mechanisms associated with these conditions are remarkably complex [7, 37]. A comprehensive comprehension of the regulatory pathways governing retinal lipid metabolism is crucial for deciphering the pathogenesis of these disorders.

Serval studies have demonstrated the impact of HFD on retinal lipid composition [38–41]. Our investigation similarly identified alterations in lipids, including phospholipids, cholesterol, and eicosanoids subsequent to HFD consumption (Fig. 3). The upregulated lipid subclasses were mainly CE, PG, and PC, suggesting that a long-term HFD increased the amount of common lipids in the retina. The eicosanoid, which was downregulated in HFM retina, plays a role in regulating the vascular, renal, and gastrointestinal, is associated with inflammatory process [42, 43], and its reduction in the HFM may impair the inflammation-related processes. Inhibitors have been developed that interfere with the synthesis or action of various classes of eicosanoid, some of which have been used to treat diseases [37].

Cholesterol homeostasis has been widely reported to be associated with the pathogenesis of glaucoma and AMD [44, 45]. Therefore, changes in the lipid composition of the retina after HFD may be important in the development of retinal diseases. HFD increases the expression and phosphorylation of NF-κB [46, 47], which is a well-known regulator of inflammatory signal transduction, false regulation of NF-κB triggers autoimmune disease, chronic inflammation, and many cancers [48]. Our findings suggest that reductions of eicosanoids in the retina may impair inflammation-related processes and that KEGG-enriched arachidonic acid metabolic pathways (Fig. 4A), which involve three major classes of enzymes related to phospholipid synthesis and eicosanoids, have been implicated in immune disorders. These studies suggest that modulation of the immune system may ameliorate some of the effects of HFD. Our proteomic KEGG was enriched to primary bile acid biosynthesis pathway (Fig. 5B), these results suggest that HFD may affect the normal function of the retina by regulating bile acid synthesis. To our surprise, the most significantly elevated proteins in HFM retinas, ACOX2, CYP27 A1, and HSD3B7 were enriched into primary bile acid biosynthesis pathway. These three proteins are enzymes that related to the synthesis of bile acids from cholesterol. Previous lipidomic analyses suggested that a long-term HFD caused an increased retinal cholesterol level, and the synthesis of bile acids is the predominant pathway by which cholesterol is eliminated from the body. Therefore the elevated expression of these three proteins may be required for the degradation of cholesterol.

Some studies have now found that HFD alters RPE morphology, leading to RPE lesions [49], RPE cell death [50], and damages microglia, retinal ganglion cells, bipolar cells, and photoreceptor cells [51]. However, the effects of HFD on different cells of the retina and the regulatory mechanisms are not known, so we performed single-cell sequencing. MG cells are the most numerous glial cells in the retina, and one of their roles is to maintain cholesterol homeostasis [52], these two types of cells may play an important role in the regulation of retinal metabolism. So, we focused on these two types of cells and analyzed the gene expression changes in these two types of cells separately. We found that the three proteins ACOX2, CYP27 A1, and HSD3B7, which were screened

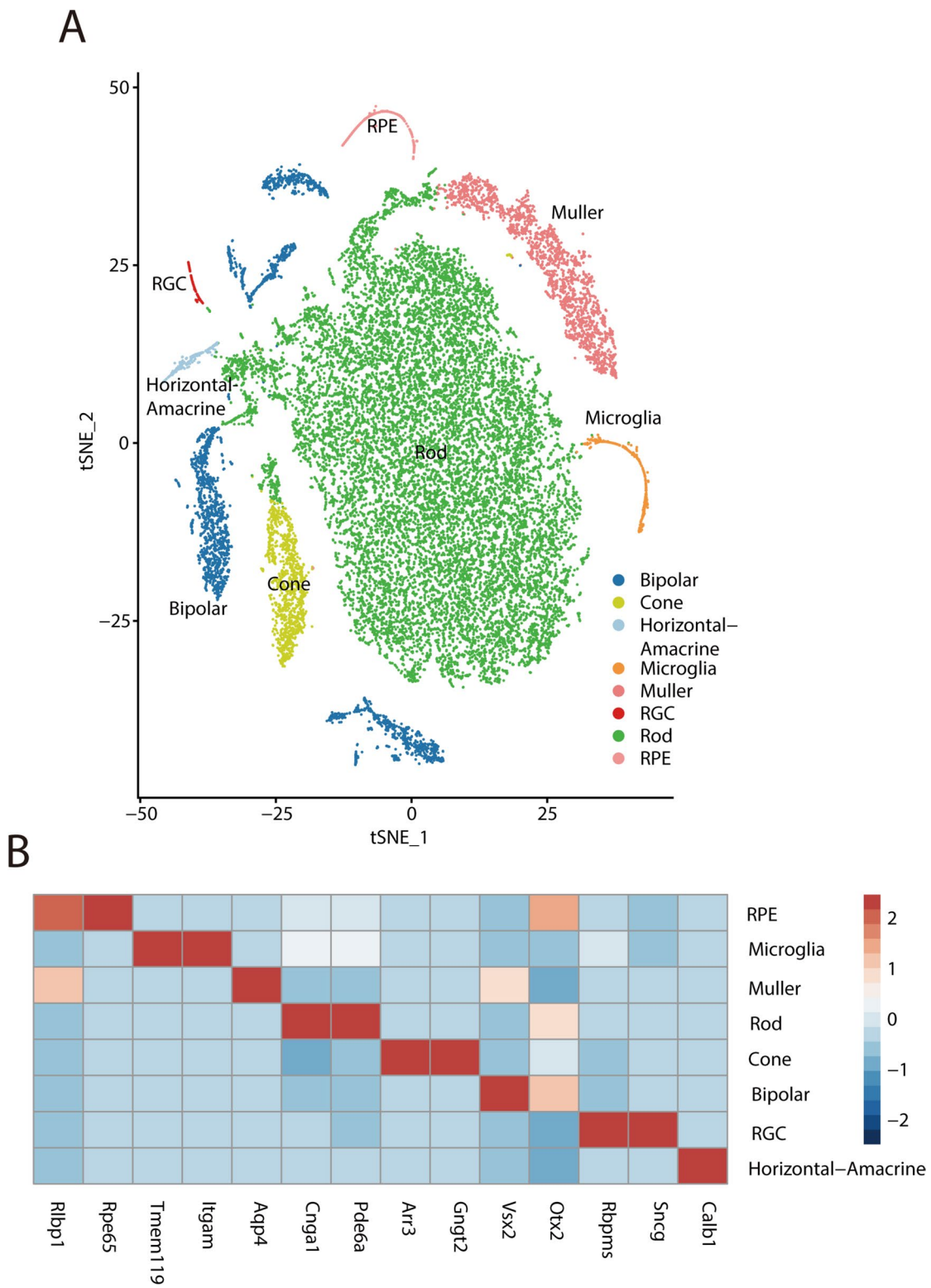

Fig. 6 Long-term HFDinduces alterations in retinal cellular composition. **A** *t*-Stochastic neighbor embedding (tSNE) plot showing the distribution of major cell populations using scRNA-seq. Using marker genes, cells were annotated as RPE, Rod, RGC, MG, Microglia, Horizon-Amacrine, Cone, and Bipolar. Colors indicate cell type. Each dot represents a cell. **B** The marker genes for each cell used are shown in the heat map

in the proteome for upregulation in the bile acid synthesis pathway, were also upregulated in MG (Fig. 7A), which further validated the possibility that HFD may affect the bile acid synthesis pathway and thus regulate cholesterol elevation in the retina due to chronic HFD. It has been reported that ACOX2 is an acyl coenzyme A oxidase, which is involved in the degradation of long branched-chain fatty acids and bile acid intermediates in peroxisomes. Deficiency of this enzyme leads to accumulation of branched-chain fatty acids and bile acid intermediates [53]. HSD3B7 is involved in the initial stages of bile acid synthesis from cholesterol and deficiency leads to cholestasis [54]. Bile acid synthesis pathways can be divided into two main categories: classical and alternative pathways.CYP27 A1 is mainly involved in the latter alternative pathway [55–57]. Our study found that the expression of these three proteins was elevated after HFD. Furthermore, a significant upregulation of CYP27 A1 expression was observed, suggesting that lipid change in the retina after HFD may be regulated by the alternative bile acid pathway and mainly in MG.

Conclusions

In summary, our findings suggest that a high-fat diet leads to changes in retinal lipid composition, where changes in cholesterol may be regulated primarily by alternative pathways of bile acid synthesis. In addition, we found a significant upregulation of CYP27 A1 in MG, suggesting that lipid change may occur mainly in MG. Our findings provide new insights and potential research directions for retinal diseases associated with lipid metabolism dysregulation, such as AMD, glaucoma, and RP.

Methods

Mouse model

All animal experiments were approved by the Animal Care and Use Committee of the Sichuan Provincial People's Hospital and were in accordance with the Declaration of Helsinki. All experimental procedures were performed in strict accordance with the approved study protocol. Mice were housed under routine light conditions with 12-h light and 12-h dark cycles and unrestricted access to food and water.

Wild-type mice of C57BL/6 J background were produced by Yao Kang Biotechnology, (Chengdu, China). Normal-fed mice (NM) were fed with normal chow for 6 months and high-fat diet mice (HFM) were fed with high-fat chow for 6 months. High-fat chow from Ready Dietech (Shenzhen, China), with 20% fat, 22% fructose, and 2% cholesterol.

Optical coherence tomography (OCT)

Mice were anesthetized with 1% sodium pentobarbital anesthetic (80 mg/kg body weight) prepared in 0.9% physiological saline [58], and tropomycin ophthalmic solution was placed on the cornea. After the pupils of the mice were dilated, OCT scanning was initiated using a phoenix micron iv (USA), and the images were acquired according to standard OCT test procedures. Calculations and processing were also performed using the accompanying image processing software.

Electroretinograms (ERGs) in mice

ERG recordings followed the previous description [59]. Briefly, age-matched NM and HFM mice were dark-adapted overnight, and all subsequent procedures were performed under dim red light. Mice were anesthetized using ketamine (16 mg/kg body weight) and chlorpromazine (80 mg/kg body weight) mixed with saline. A drop of tropicamide and phenylephrine into a mouse eye dilates the pupil. The dark-adapted ERGs of the mice in response to flashes of light with intensities ranging from 0.01 to 1.0 cd-s/m^2 were recorded using the Espion visual electrophysiology system (Diagnosys LLC, Littleton, MA, USA). Four NM mice and 4 HFM mice were tested in each group.

Single-cell transcriptomic analysis

Sample processing and collection

Retinas were removed from euthanized mice by intraperitoneal injection of pentobarbital (80 mg/kg) and by cervical dislocation, rinsed with PBS, and then the tissues were moved into tissue storage solution separately and sent to Juyuan Genetic Technology Co. (Chengdu, Sichuan) for further processing. Tissues were flushed with PBS and digested with papain (1 mg/ml) for 15 min at 37 °C. Products were filtered with 40-μm sieve, centrifugated at 500 ×*g* for 5 min, resuspended in PBS, and stained with Tapan Blue for microscopic examination. The concentration of single cell is more than 1× 10^6cell/

(See figure on next page.)

Fig. 7 Different regulation of gene expression in MG and rod cells in a high-fat environment. **A** The heatmap shows the expression changes in different cells of the most changed genes screened by proteomic analysis. **B** Dot plot of expression levels of Acox2, Cyp27a1, and Hsd3b7 in MG cells. **C** KEGG pathway analysis of the DEGs in MG cells enriched in different pathways, showing the top 10 ranked pathways. **D** KEGG pathway analysis of the DEGs in Rod cells enriched in different pathways, showing the top 10 ranked pathways. **E** Chord diagram shows the relationship between DEGs and KEGG pathways in MG cells. **F** Chord diagram shows the relationship between DEGs and KEGG pathways in Rod cells

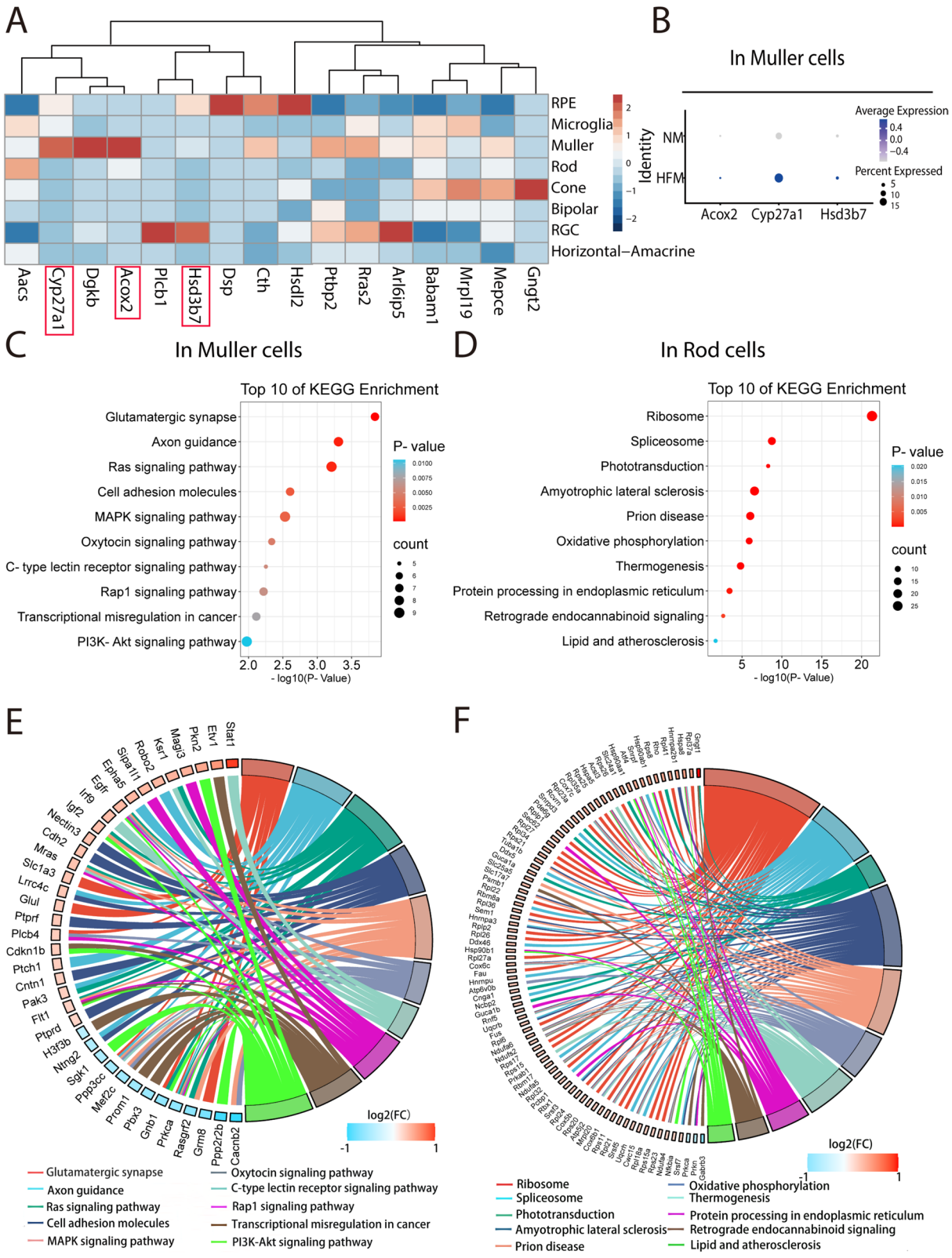

Fig. 7 (See legend on previous page.)

mL, and the cell activity is more than 85%, then library construction and sequencing.

Single-cell transcriptomic data analysis

The data were analyzed with the same methods as previously described [60]. Briefly, The analysis utilized Seurat software version 4.3.0 for processing count data obtained from scRNA-seq [61]. Cells exhibiting fewer than 200 or more than 2000 detected genes were excluded from the dataset. Additionally, cells demonstrating a high proportion of reads originating from mitochondrial genes (> 15%) were removed due to potential issues related to cell viability or data quality. Integration of data from NM and HFM groups was conducted using Seurat's "anchor-based" integration workflow with dimensions set to 1:30 [62]. Subsequently, the count matrix underwent normalization using the LogNormalize method. Clustering was conducted at a resolution of 1 using PCA-reduced expression data derived from the top 20 principal components. The graph-based shared nearest neighbor method (SNN) was employed, which computes the neighborhood overlap (Jaccard index) between each cell and its closest neighbors. Clustered populations were visualized using *t*-distributed stochastic neighbor embedding (*t*-SNE). Each cell population was assigned based on the expression of specific marker genes, including Rlbp1 and RPE65 for RPE, Tmem119 and Itgam for microglia, Aqp4 for Müller cells, Cnga1 and Pde6a for rod photoreceptors, Arr3 and Gngt2 for cone photoreceptors, Vsx2 and Otx2 for bipolar cells, and Rbpms and Sncg for RGCs. Due to their limited abundance, horizontal and amacrine cells were clustered together, characterized by the expression of Calb1. Differentially expressed genes (DEGs) between distinct cell types under two conditions (NM vs HFM) were identified using the FindMarkers function. Screening thresholds for significant differential expression were set at adjusted-*P* values < 0.05 and Fold change (FC) > 1.5.

KEGG pathway enrichment analyses of DEGs were done using R based on hypergeometric distributions. R-studio (version 1.4.1106) was used to run all R packages and functions in this study, and all procedures followed established procedures.

Proteomic analysis

Sample processing and collection

Retinas and livers were taken from three 6-month-old high-fat mice and three normal-diet mice by intraperitoneal injection of pentobarbital (80 mg/kg) and by cervical dislocation, and appropriate amount of SDT lysate was added, transferred to Lysing Matrix A tubes, and homogenized and broken by applying an MP homogenizer (24 ×2, 6.0 M/S, 30 s, twice). After sonication, boiling water bath for 10 min, centrifugating at 14,000 ×*g* for 15 min, the supernatant was taken and filtered using a 0.22-μm centrifuge tube and the filtrate was collected. The filtrate was quantified with the BCA Protein Assay Kit (P0012, Beyotime). The samples were divided and stored at − 80 °C.

Protein preparation

Fifty to two hundred micrograms of proteins for each sample was reduced with DTT (100 mM) for 5 min at 100℃. UA buffer (8 M Urea, 150 mM Tris–HCl pH 8.5) was added and mixed, transferred to a 30-kD ultrafiltration centrifuge tube to remove detergent, DTT, and other low molecular weight components. IAA buffer (100 mM IAA in UA) was added to block reduced cysteine residues and the samples were incubated at room temperature for 30 min. Finally, the protein suspension was digested with 4 μg of trypsin (Promega) in 40 μl of 50 mM NH4HCO3 buffer overnight at 37 °C, and the peptides were collected in the filtrate. The peptides were desalted by C18 Cartridge, lyophilized, and reconstituted in 40 μL of 0.1% formic acid solution, and quantified (OD280).

Mass spectrometry

The samples were separated using a nanoliter flow rate NanoElutesystem (Bruker, Bremen, Germany), which was coupled to a mass spectrometer timsTOF Pro(Bruker, Bremen, Germany) equipped with a CaptiveSpray ion source. Buffer solution A was 0.1% formic acid aqueous solution and solution B was 0.1% formic acid acetonitrile aqueous solution (100% acetonitrile). The column was equilibrated with 100% of solution A. Samples were uploaded by an autosampler to an analytical column (IonOpticks, Australia, 25 cm ×75 μm, C18 packing 1.6 μm) for separation at a flow rate of 300 nL/min. The samples were separated by chromatography and analyzed by mass spectrometry using the PASEF mode of a timsTOF Pro mass spectrometer.

Proteomic data analysis

In this paper, MaxQuant software (version no. 1.6.17.0) was used for database search and LFQ (Label Free Quantitation) algorithm was used for quantitative analysis. Signaling pathway analysis was performed using the KEGG database (database version KO_INFO_END.txt (2023.03.24)) for pathway analysis. KEGG pathways with adjusted *P*-value less than 0.05 calculated by hypergeometric test and Benjamini–Hochberg method can be defined as significantly enriched pathways. The top 10 enriched pathways were selected for visualization.

Lipidome analysis

Sample processing and collection

Retinas from three 6-month-old high-fat mice and three mice of the same age on a normal diet were weighed and 20 mg was added to a 2-mL centrifuge tube; 1 mL of lipid extraction solution was added, and the balls were placed in the tubes, and shaken well; homogenization was performed in a ball mill; the balls were removed; vortexing was performed for 2 min, and ultrasound was performed for 5 min, and 200 µL of water was added; the tubes were vortexed for 1 min, and the supernatant was centrifuged for 10 min at 12,000 ×*g* and 4 ℃. Centrifugation was done for 10 min at 12,000 ×*g* at 4 ℃. Two hundred microliters of the supernatant was pipetted into a numbered 1.5-mL centrifuge tube and concentrate; the supernatant was reconstituted with 200 µL of the lipid reagent solution and used it for LC–MS/MS analysis.

The data acquisition instrumentation system consists primarily of Ultra Performance Liquid Chromatography (UPLC) (ExionLC™ AD, https://sciex.com.cn/)and Tandem Mass Spectrometry (MS/MS) (QTRAP® 6500 +, https://sciex.com.cn/).

The liquid phase conditions mainly included: (1) column: Thermo Accucore™C30 column (2.6 µm, 2.1 mm ×100 mm i.d.); (2) mobile phases: phase A, acetonitrile/water (60/40, V/V) (containing 0.1% formic acid, 10 mmol/L ammonium formate); phase B, acetonitrile/isopropanol (10/90, V/V) (containing 0.1% formic acid, 10 mmol/L ammonium formate); (3) gradient elution program: 80:20 (V/V) for A/B at 0 min, 70:30 (V/V) at 2 min, 40:60 (V/V) at 4 min, 15:85 (V/V) at 9 min, 10:90 (V/V) at 14 min, 5:95 (V/V) at 15.5 min, 5:95 (V/V) at 17.3 min. 17.5 min for 80:20 (V/V), and 20 min for 80:20 (V/V); (4) flow rate of 0.35 ml/min; column temperature of 45 ℃; injection volume of 2 µL.

The mass spectrometry conditions mainly included: electrospray ionization (ESI) temperature 500 ℃, mass spectrometry voltage 5500 V in positive ion mode, mass spectrometry voltage −4500 V in negative ion mode, ion source gas 1 (GS1) 45 psi, gas 2 (GS2) 55 psi, Curtain Gas (CUR) 35 psi. In the triple quadrupole, each ion pair was scanned based on optimized declustering potential (DP) and collision energy (CE).

Detection of lipids was done as follows: lipid contents were detected by MetWare (http://www.metware.cn/) based on the AB Sciex QTRAP 6500 LC–MS/MS platform [63].

Lipidome data analysis

Mass spectrometry data were processed using the software Analyst 1.6.3. The lipids of the samples were characterized by mass spectrometry based on the data information of the self-constructed database MWDB (metware database). The integrated peak area ratios of all the samples detected were substituted into the linear equation for calculation, and further brought into the calculation formula for calculation to finally obtain the content data of the substance in the actual samples. Lipids with VIP (Variable Importance in Projection) >1 and *P*-value <0.05 were selected for differential lipid screening.

The identified metabolites were annotated using the KEGG Compound Database (http://www.kegg.jp/kegg/compound/), and the annotated metabolites were then mapped to the KEGG pathway database (http://www.kegg.jp/kegg/pathway.html). The significantly regulated pathways to which the metabolites were mapped were then entered into MSEA (metabolite set enrichment analysis) and their significance was determined by *P*-values from hypergeometric tests [64].

Statistical analysis

Statistical analysis was performed using the GraphPad Prism 8.0.2 software. All data are presented as the mean ± standard error of mean (SEM). Statistical significance was determined by unpaired Student's *t* test. *P*-value lower than 0.05 ($P < 0.05$) was considered to indicate statistical significance.

Abbreviations

BA	Bile acids
BMP	Bis monoacylglycero phosphate
CAR	Ceramide
CE	Cholesterol esterase
Cer-AP	Ceramide AP
Cer-AS	Ceramide with Stearic Acid
Cer-NDS	Ceramide with N-acyl-D-sphingosine
Cer-NP	Ceramide with N-palmitoyl
Cer-NS	Ceramide with N-acyl-sphingosine
CerP	Ceramide Phosphate
CoQ	Coenzyme Q
DG	Diacylglycerol
DG-O	Monoacylglycerol ether
FFA	Free fatty acids
Hex2 Cer	Hexosylceramide (with two hexose sugars)
HexCer-AP	Hexosylceramide with arachidonic acid
HexCer-NS	Hexosylceramide with N-acyl-sphingosine
LNAPE	Lysophosphatidylethanolamine
LPA	Lysophosphatidic acid
LPC	Lysophosphatidylcholine
LPC-O	Lysophosphatidylcholine ether
LPE	Lysophosphatidylethanolamine
LPE-P	Phosphorylated lysophosphatidylethanolamine
LPG	Lysophosphatidylglycerol
LPI	Lysophosphatidylinositol
LPS	Lysophosphatidylserine
MG	Monoglyceride
MGDG	Monogalactosyldiacylglycerol
PC	Phosphatidylcholine
PC-O	Phosphatidylcholine ether
PE	Phosphatidylethanolamine
PE-O	Phosphatidylethanolamine ether
PE-P	Phosphatidylethanolamine phosphate
PG	Phosphatidylglycerol

PI	Phosphatidylinositol
PMeOH	Phosphatidylmethanol
PS	Phosphatidylserine
SHexCer	Sulfated hexosylceramide
SM	Sphingomyelin
SPH	Sphingosine
TG	Triglyceride

Supplementary Information

The online version contains supplementary material available at https://doi.org/10.1186/s12915-025-02212-z.

Additional file 1: Fig S1. High-fat diet mouse model construction. Fig S2. Proteomics reveals significantly different gene expression alterations in liver with an HFD.

Additional file 2: Table S1. Lipids Expression Results of Retinas from NM and HFM. Table S2. Protein Expression Results from 4D Label-Free Proteomic Analysis of Retinas from NM and HFM. Table S3. Protein Expression Results from 4D Label-Free Proteomic Analysis of Livers from NM and HFM. Table S4. Key resources table.

Additional file 3. Uncropped blots. The raw blots corresponding with Fig. 5D are shown with molecular weight indicators.

Acknowledgements
Not applicable

Authors' contributions
L.Z., XJ.Z., and H.Q. designed and supervised the study. R.Z. and JR.C. performed the majority of the experiments. TY.C. and WH.M. were responsible for animal breeding and genotyping. R.Z. and L.Z. wrote the manuscript. All authors read and approved the final manuscript.

Funding
This study was supported by: The National Natural Science Foundation of China (82071009, 82301231), the Department of Science and Technology of Qinghai Province (2022-HZ-814), programs from the Department of Science and Technology of Sichuan Province (2023YFS0038). The funders had no role in the study design, data collection and analysis, or preparation of the manuscript.

Data availability
All data generated or analyzed during this study are included in this published article, its supplementary information files and publicly available repositories. The dataset for the single-cell sequencing is available in the NCBI with accession PRJNA1181314. The mass spectrometry proteomics data have been deposited to the ProteomeXchange Consortium (https://proteomecentral.proteomexchange.org) via the iProX partner repository with the dataset identifier PXD052242.

Declarations

Ethics approval and consent to participate
All animal experiments were approved by the Animal Care and Use Committee of Sichuan Provincial People's Hospital (2023-46).

Consent for publication
Not applicable.

Competing interests
The authors declare that they have no competing interests.

Received: 23 April 2024 Accepted: 9 April 2025
Published online: 17 April 2025

References

1. Causes of blindness and vision impairment in 2020 and trends over 30 years, and prevalence of avoidable blindness in relation to VISION 2020: the Right to Sight: an analysis for the Global Burden of Disease Study [J]. Lancet Glob Health. 2021;9(2):e144-e160.
2. Fricke TR, Tahhan N, Resnikoff S, et al. Global Prevalence of Presbyopia and Vision Impairment from Uncorrected Presbyopia: Systematic Review, Meta-analysis, and Modelling [J]. Ophthalmology. 2018;125(10):1492–9.
3. Burton MJ, Ramke J, Marques AP, et al. The Lancet Global Health Commission on Global Eye Health: vision beyond 2020 [J]. Lancet Glob Health. 2021;9(4):e489–551.
4. Vecino E, Rodriguez F D, Ruzafa N, et al. Glia-neuron interactions in the mammalian retina [J]. Prog Retin Eye Res. 2016;51:1–40.
5. Cowan C S, Renner M, De Gennaro M, et al. Cell Types of the Human Retina and Its Organoids at Single-Cell Resolution [J]. Cell. 2020;182(6):1623–40.
6. Mutlu AS, Duffy J, Wang MC. Lipid metabolism and lipid signals in aging and longevity [J]. Dev Cell. 2021;56(10):1394–407.
7. Farnoodian M, Bose D, Barone F, et al. Retina and RPE lipid profile changes linked with ABCA4 associated Stargardt's maculopathy [J]. Pharmacol Ther. 2023;249:108482.
8. Zhao T, Guo X, Sun Y. Iron Accumulation and Lipid Peroxidation in the Aging Retina: Implication of Ferroptosis in Age-Related Macular Degeneration [J]. Aging Dis. 2021;12(2):529–51.
9. Salazar J, Olivar LC, Ramos E, et al. Dysfunctional High-Density Lipoprotein: An Innovative Target for Proteomics and Lipidomics [J]. Cholesterol. 2015;2015:296417.
10. Marcus MW, Müskens RPHM, Ramdas WD, et al. Cholesterol-lowering drugs and incident open-angle glaucoma: a population-based cohort study [J]. PLoS ONE. 2012;7(1):e29724.
11. Yang J, Chen Y, Zou T, et al. Cholesterol homeostasis regulated by ABCA1 is critical for retinal ganglion cell survival [J]. Sci China Life Sci. 2023;66(2):211–25.
12. Newman-Casey PA, Talwar N, Nan B, et al. The relationship between components of metabolic syndrome and open-angle glaucoma [J]. Ophthalmology. 2011;118(7):1318–26.
13. Nusinovici S, Li H, Thakur S, et al. High-Density Lipoprotein 3 Cholesterol and Primary Open-Angle Glaucoma: Metabolomics and Mendelian Randomization Analyses [J]. Ophthalmology. 2022;129(3):285–94.
14. Woudberg NJ, Pedretti S, Lecour S, et al. Pharmacological Intervention to Modulate HDL: What Do We Target? [J]. Front Pharmacol. 2017;8:989.
15. Gordon SM, Deng J, Tomann AB, et al. Multi-dimensional co-separation analysis reveals protein-protein interactions defining plasma lipoprotein subspecies [J]. Mol Cell Proteomics. 2013;12(11):3123–34.
16. Lin H-C, Chien C-W, Hu C-C, et al. Comparison of comorbid conditions between open-angle glaucoma patients and a control cohort: a case-control study [J]. Ophthalmology. 2010;117(11):2088–95.
17. Wang S, Bao X. Hyperlipidemia, Blood Lipid Level, and the Risk of Glaucoma: A Meta-Analysis [J]. Invest Ophthalmol Vis Sci. 2019;60(4):1028–43.
18. Mcgwin G, Mcneal S, Owsley C, et al. Statins and other cholesterol-lowering medications and the presence of glaucoma [J]. Arch Ophthalmol. 2004;122(6):822–6.
19. Owen CG, Carey IM, Shah S, et al. Hypotensive medication, statins, and the risk of glaucoma [J]. Invest Ophthalmol Vis Sci. 2010;51(7):3524–30.
20. Liu L, Zhang K, Sandoval H, et al. Glial lipid droplets and ROS induced by mitochondrial defects promote neurodegeneration [J]. Cell. 2015;160(1–2):177–90.
21. Van Den Brink DM, Cubizolle A, Chatelain G, et al. Physiological and pathological roles of FATP-mediated lipid droplets in Drosophila and mice retina [J]. PLoS Genet. 2018;14(9):e1007627.
22. Zhang Y, Huang J, Liang Y, et al. Clearance of lipid droplets by chimeric autophagy-tethering compound ameliorates the age-related macular degeneration phenotype in mice lacking APOE [J]. Autophagy. 2023;19(10):2668–81.
23. Kim S, Stockwell A, Qin H, et al. Rare CIDEC coding variants enriched in age-related macular degeneration patients with small low-luminance deficit cause lipid droplet and fat storage defects [J]. PLoS ONE. 2023;18(4):e0280484.
24. Tsai Y-T, Li Y, Ryu J, et al. Impaired cholesterol efflux in retinal pigment epithelium of individuals with juvenile macular degeneration [J]. Am J Hum Genet. 2021;108(5):903–18.

25. Lyu J, Chen Y, Yang W, et al. The conserved microRNA miR-210 regulates lipid metabolism and photoreceptor maintenance in the Drosophila retina [J]. Cell Death Differ. 2021;28(2):764–79.
26. Schlegel D K, Ramkumar S, Von Lintig J, et al. Disturbed retinoid metabolism upon loss of rlbp1a impairs cone function and leads to subretinal lipid deposits and photoreceptor degeneration in the zebrafish retina [J]. Elife. 2021;10:e71473.
27. Muliyil S, Levet C, Düsterhöft S, et al. ADAM17-triggered TNF signalling protects the ageing Drosophila retina from lipid droplet-mediated degeneration [J]. EMBO J. 2020;39(17):e104415.
28. Kutsyr O, Noailles A, Martínez-Gil N, et al. Short-term high-fat feeding exacerbates degeneration in retinitis pigmentosa by promoting retinal oxidative stress and inflammation [J]. Proc Natl Acad Sci U S A. 2021;118(43):e2100566118.
29. Zou R. High-fat diet alters retinal gene expression networks in mice. 2024. ProteomeXchange Consortium via the PRIDE partner repository with the dataset identifier PXD052242. https://proteomecentral.proteomexchange.org/ui.
30. Andraski A B, Singh S A, Higashi H, et al. The distinct metabolism between large and small HDL indicates unique origins of human apolipoprotein A4 [J]. JCI Insight. 2023;8(8):e162481.
31. Lu H, Wang B, Liu Y, et al. DiLeu Isobaric Labeling Coupled with Limited Proteolysis Mass Spectrometry for High-Throughput Profiling of Protein Structural Changes in Alzheimer's Disease [J]. Anal Chem. 2023;95(26):9746–53.
32. Carter CJ. Convergence of genes implicated in Alzheimer's disease on the cerebral cholesterol shuttle: APP, cholesterol, lipoproteins, and atherosclerosis [J]. Neurochem Int. 2007;50(1):12–38.
33. Lin Q, Cao Y, Gao J. Decreased expression of the APOA1-APOC3-APOA4 gene cluster is associated with risk of Alzheimer's disease [J]. Drug Des Devel Ther. 2015;9:5421–31.
34. Eisen JA. A phylogenomic study of the MutS family of proteins [J]. Nucleic Acids Res. 1998;26(18):4291–300.
35. Zhou T, Chen L, Huang C-H, et al. Serine Proteinase Inhibitor SERPINA3K Suppresses Corneal Neovascularization via Inhibiting Wnt Signaling and VEGF [J]. Invest Ophthalmol Vis Sci. 2014;55:4863–72.
36. Zou R. High-fat diet alters retinal lipid composition and gene expression networks in mice. 2024. GenBank. https://www.ncbi.nlm.nih.gov/sra/PRJNA1181314.
37. Fu Z, Chen CT, Cagnone G, et al. Dyslipidemia in retinal metabolic disorders [J]. EMBO Mol Med. 2019;11(10):e10473.
38. Dai W, Dierschke SK, Toro AL, et al. Consumption of a high fat diet promotes protein O-GlcNAcylation in mouse retina via NR4A1-dependent GFAT2 expression [J]. Biochim Biophys Acta Mol Basis Dis. 2018;1864(12):3568–76.
39. Dai W, Miller W P, Toro A L, et al. Deletion of the stress-response protein REDD1 promotes ceramide-induced retinal cell death and JNK activation [J]. FASEB J. 2018;32(12):fj201800413RR.
40. Chang RC-A, Shi L, Huang CC-Y, et al. High-Fat Diet-Induced Retinal Dysfunction [J]. Invest Ophthalmol Vis Sci. 2015;56(4):2367–80.
41. Atawia RT, Bunch KL, Fouda AY, et al. Role of Arginase 2 in Murine Retinopathy Associated with Western Diet-Induced Obesity [J]. J Clin Med. 2020;9(2):317.
42. Calder PC. Eicosanoids [J]. Essays Biochem. 2020;64(3):423–41.
43. Christie WW, Harwood JL. Oxidation of polyunsaturated fatty acids to produce lipid mediators [J]. Essays Biochem. 2020;64(3):401–21.
44. Kolko M, Mouhammad ZA, Cvenkel B. Is fat the future for saving sight? Bioactive lipids and their impact on glaucoma [J]. Pharmacol Ther. 2023;245:108412.
45. Pikuleva IA, Curcio CA. Cholesterol in the retina: the best is yet to come [J]. Prog Retin Eye Res. 2014;41:64–89.
46. Lee J-J, Wang P-W, Yang IH, et al. High-fat diet induces toll-like receptor 4-dependent macrophage/microglial cell activation and retinal impairment [J]. Invest Ophthalmol Vis Sci. 2015;56(5):3041–50.
47. Chen X, Wang X, Zhou X. Pseudophakic ametropia management with toric implantable collamer lens with a central hole (case report) [J]. BMC Ophthalmol. 2017;17(1):17.
48. Hayden MS, Ghosh S. Shared principles in NF-kappaB signaling [J]. Cell. 2008;132(3):344–62.
49. Filas BA, Zhang Q, Okamoto RJ, et al. Enzymatic degradation identifies components responsible for the structural properties of the vitreous body [J]. Invest Ophthalmol Vis Sci. 2014;55(1):55–63.
50. Roddy GW, Rosa RH, Viker KB, et al. Diet Mimicking "Fast Food" Causes Structural Changes to the Retina Relevant to Age-Related Macular Degeneration [J]. Curr Eye Res. 2020;45(6):726–32.
51. Clarkson-Townsend DA, Douglass AJ, Singh A, et al. Impacts of high fat diet on ocular outcomes in rodent models of visual disease [J]. Exp Eye Res. 2021;204:108440.
52. Gambert S, Gabrielle P-H, Masson E, et al. Cholesterol metabolism and glaucoma: Modulation of Muller cell membrane organization by 24S-hydroxycholesterol [J]. Chem Phys Lipids. 2017;207(Pt B):179–91.
53. O'sullivan É, Keogh A, Henderson B, et al. Treatment Strategies for KRAS-Mutated Non-Small-Cell Lung Cancer [J]. Cancers (Basel). 2023;15(6):1635.
54. Zhao J, Setchell KDR, Gong Y, et al. Genetic spectrum and clinical characteristics of 3β-hydroxy-Δ5-C27-steroid oxidoreductase (HSD3B7) deficiency in China [J]. Orphanet J Rare Dis. 2021;16(1):417.
55. Baek AE, Yu Y-RA, He S, et al. The cholesterol metabolite 27 hydroxycholesterol facilitates breast cancer metastasis through its actions on immune cells [J]. Nat Commun. 2017;8(1):864.
56. Chiang JYL, Ferrell JM. Bile Acid Metabolism in Liver Pathobiology [J]. Gene Expr. 2018;18(2):71–87.
57. Ticho AL, Malhotra P, Dudeja PK, et al. Intestinal Absorption of Bile Acids in Health and Disease [J]. Compr Physiol. 2019;10(1):21–56.
58. Pang D, Laferriere C. Review of Intraperitoneal Injection of Sodium Pentobarbital as a Method of Euthanasia in Laboratory Rodents [J]. J Am Assoc Lab Anim Sci. 2020;59(3):346.
59. Li X, Jiang Z, Su Y, et al. Deletion of Emc1 in photoreceptor cells causes retinal degeneration in mice [J]. FEBS J. 2023;290(17):4356–70.
60. Liu B, He J, Zhong L, et al. Single-cell transcriptome reveals diversity of Müller cells with different metabolic-mitochondrial signatures in normal and degenerated macula [J]. Front Neurosci. 2022;16:1079498.
61. Hao Y, Hao S, Andersen-Nissen E, et al. Integrated analysis of multimodal single-cell data [J]. Cell. 2021;184(13):3573–87.
62. Stuart T, Butler A, Hoffman P, et al. Comprehensive Integration of Single-Cell Data [J]. Cell. 2019;177(7):1888–902.
63. Xuan Q, Hu C, Yu D, et al. Development of a High Coverage Pseudotargeted Lipidomics Method Based on Ultra-High Performance Liquid Chromatography-Mass Spectrometry [J]. Anal Chem. 2018;90(12):7608–16.
64. Thévenot EA, Roux A, Xu Y, et al. Analysis of the Human Adult Urinary Metabolome Variations with Age, Body Mass Index, and Gender by Implementing a Comprehensive Workflow for Univariate and OPLS Statistical Analyses [J]. J Proteome Res. 2015;14(8):3322–35.

Publisher's Note